in patients with newly diagnosed MGs (Fig. 4). When this group was subdivided, the PFS rate at 12 months was 55.6% (95% CI: 20.4–80.5%) in the GBM group and 71.4% (95% CI: 25.8–92.0%) in the non-GBM group. For patients with recurrent MGs, the PFS rate at 6 months was 37.5% (95% CI: 8.7–67.4%), the PFS rate at 12 months was 25.0% (95% CI: 3.7–55.8%), and the median PFS was 170 days (Fig. 4). When this group was subdivided, the PFS rates at 6 months and 12 months were both 25.0% (95% CI: 0.9–66.5%) in the GBM group and 50.0% (95% CI: 5.8–84.5%) in the non-GBM group. Figure 5 shows gadolinium contrast-enhanced T_1 MRIs before insertion, within 3 days of insertion, and 6 months and 12 months after insertion of BCNU implants in a patient with recurrent GBM (first relapse). A tumor, 5 cm in size, was noted in the left frontal lobe, and 8 sheets of the BCNU implant were inserted. Subsequently, TMZ alone (220–260 mg/day) was applied for 9 cycles. Even at 12 months after insertion, there was no tumor growth or any other changes observable on MRI images.

During this study, non-responders to TMZ received either BEV therapy (1 newly diagnosed GBM patient and 1 recurrent GBM patient) or IMRT therapy (1 recurrent anaplastic astrocytoma patient). BEV therapy for the newly diagnosed GBM patient involved 5 cycles of treatment (330 mg/day) after recurrence at 8.4 months after insertion of BCNU implants. The patient died 12 months (362 days) after insertion of the BCNU implants. BEV therapy for the second recurrence GBM patient involved 10 cycles of treatment (500 mg/day) at 5.7 months after insertion of the BCNU implants. The patient died at 18.2 months (546 days) after insertion of the BCNU implants. IMRT therapy was applied at a dose of 60 Gy to the enhanced area and 50 Gy to the area around the lesion after the second recurrence at 7.3 months after insertion of

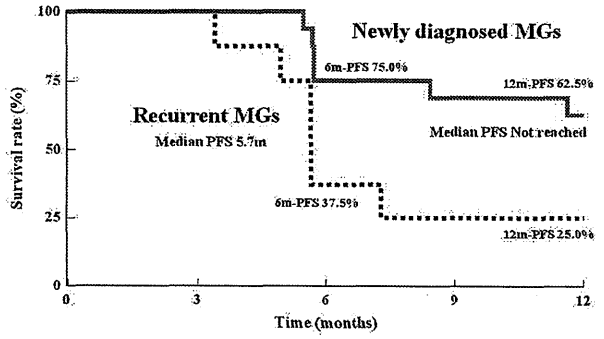

Fig. 4 Kaplan-Meier curve of progression-free survival period/rate (judged by the efficacy and safety evaluation committee). MGs: malignant gliomas, PFS: progression-free survival rate, m: months, 6m-PFS: progression-free survival rate at 6 months, 12m-PFS: progression-free survival rate at 12 months.

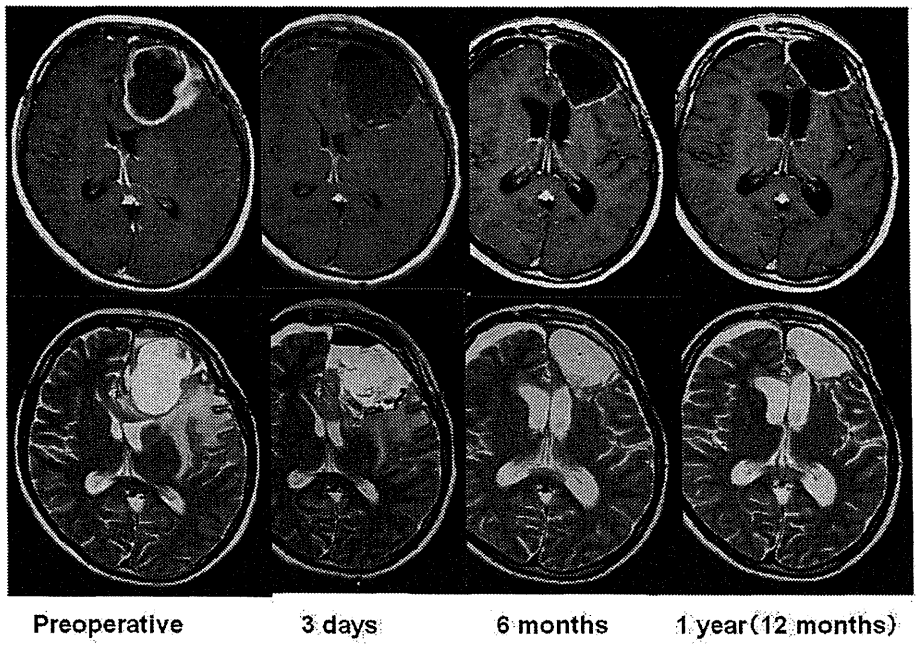

Fig. 5 Time course of magnetic resonance (MR) imaging findings (1st relapse of recurrent glioblastoma), axial gadolinium contrast-enhanced T_1-weighted MR images (*upper row*), and T_2-weighted MR images (*lower row*).

the BCNU implants. The patient died at 16.1 months (483 days) after insertion of the BCNU implants.

II. Safety

Adverse events were noted in 24 of 24 (100%) patients who received BCNU implants and adverse events attributable to BCNU implants were 13 of 24 patients (54.2%). Major adverse events (over 20%, Table 2) listed in descending order of incidence were fever (18 cases, 75.0%); alopecia (16 cases, 66.7%); constipation (14 cases, 58.3%); headache (13 cases, 54.2%); nausea (12 cases, 50.0%), wound complication and leukocytopenia (11 cases each, 45.8%); brain neoplasm (10 cases, 41.7%); vomiting, malaise, brain edema, and lymphopenia (9 cases each, 37.5%); anorexia and hemiparesis (8 cases each, 33.3%); insomnia (7 cases, 29.2%); aphasia, seizure, and increase in blood creatine phosphokinase (CPK; 6 cases each, 25.0%); and pruritus, facial swelling, radiation-induced skin injury, and weight loss (5 cases each, 20.8%). Of these adverse events, severe events (grade 3) included brain neoplasm (7 cases, 29.2%), hemiplegia (6 cases, 25.0%), brain edema (4 cases, 16.7%), and aphasia (3 cases, 12.5%). Adverse, life-threatening events or those causing disabilities (grade 4) included tumor progression (3 cases, 4.2%).

Within 12 months (360 days) of BCNU implant insertion, 3 patients died from tumor progression. None of the deaths had causal relationships with the investigational drug. Within 24 months of BCNU implant insertion, 6 patients died in addition to the above-mentioned 3 patients (9 deaths in total). The cause of death was progressive disease (PD) in 5 cases (2 newly diagnosed MGs and 3 recurrent MGs) and respiratory failure in 1 case (newly diagnosed MG). None of these deaths had causal relationships with the investigational drug.

Frequently noted adverse events attributable to BCNU implants (adverse reactions, Table 3) were brain edema (6 cases, 25.0%); fever and lymphocytopenia (3 cases each, 12.5%); and nausea, vomiting, headache, hemiparesis, anorexia, and increase in alanine aminotransferase (ALT; 2 cases each, 8.3%). None of these adverse reactions were rated as grade 4 or worse. There were 6 cases of grade 3 events in 5 of 24 patients (20.8%) including brain edema (2 cases), hemiparesis (2 cases), increase in ALT (1 case), and increase in CPK (1 case). None of the patients experienced convulsion, poor wound healing, infection, meningitis, or hydrocephalus as an adverse reaction. The adverse reactions listed above appeared within 3 months of BCNU implant insertion.

Among the patients who did not respond to TMZ and who received BEV therapy (1 newly diagnosed

Table 2 Number of patients (%) who experienced adverse events according to Common Terminology Criteria for Adverse Events (CTCAE) grade (events with an incidence over 20%)

System organ class/event name	Cases (%) (n = 24)			
	All grades		Grade 3 or higher	
All adverse events	24	(100.0)	19	(79.2)
Gastrointestinal disorders				
Nausea	12	(50.0)		–
Constipation	14	(58.3)		–
Vomiting	9	(37.5)		–
General disorders and administration site conditions				
Malaise	9	(37.5)		–
Fever	18	(75.0)	1	(4.2)
Injury, poisoning, and procedural complications				
Wound complication	11	(45.8)		–
Nervous system disorders				
Aphasia	6	(25.0)	3	(12.5)
Headache	13	(54.2)		–
Brain edema	9	(37.5)	4	(16.7)
Hemiparesis	8	(33.3)	6	(25.0)
Seizure	6	(25.0)	1	(4.2)
Psychiatric disorders				
Insomnia	7	(29.2)		–
Metabolism and nutrition disorders				
Anorexia	8	(33.3)		–
Skin and subcutaneous disorders				
Pruritus	5	(20.8)		–
Facial swelling	5	(20.8)		–
Alopecia	16	(66.7)		–
Radiation-induced skin injury	5	(20.8)		–
Neoplasms (benign, malignant, and unspecified)				
Brain neoplasm	10	(41.7)	7	(29.2)
Investigations				
Lymphopenia	9	(37.5)	2	(8.3)
Blood creatine phosphokinase increased	6	(25.0)	2	(8.3)
Weight loss	5	(20.8)		–
Leukocytopenia	11	(45.8)	2	(8.3)

MedDRA/J Version 14.0. Event name: The same event name seen in the same patient was counted as one case. If severity differed between multiple episodes of the same event, then the most severe episode was selected. System organ class: If there were multiple event names within the same system organ class in the same patient in one line, the patient was counted as one. Incidence (%) = No. of patients developing the event/All patients studied × 100.

Table 3 Number of patients (%) who attributable to BCNU implants according to Common Terminology Criteria for Adverse Events (CTCAE) grade

System organ class/event name	Cases (%) (n = 24)			
	All grades		Grade 3 or higher	
All adverse reactions	13	(54.2)	5	(20.8)
Gastrointestinal disorders				
Nausea	2	(8.3)		–
Abdominal discomfort	1	(4.2)		–
Vomiting	2	(8.3)		–
General disorders and administration site conditions				
Hypothermia	1	(4.2)		–
Fever	3	(12.5)		–
Edema	1	(4.2)		–
Nervous system disorders				
Hyperesthesia	1	(4.2)		–
Memory disorder	1	(4.2)		–
Aphasia	1	(4.2)		–
Heterotropia	1	(4.2)		–
Headache	2	(8.3)		–
Homonymous hemianopsia	1	(4.2)		–
Urinary incontinence	1	(4.2)		–
Brain edema	6	(25.0)	2	(8.3)
Monoparesis	1	(4.2)		–
Hemiparesis	2	(8.3)	2	(8.3)
Hemiplegia	1	(4.2)		–
Reproductive system and breast disorders				
Irregular menstruation	1	(4.2)		–
Metabolism and nutrition disorders				
Anorexia	2	(8.3)		–
Investigations				
C-reactive protein increased	1	(4.2)		–
Alanine aminotransferase increasd	2	(8.3)	1	(4.2)
Lymphocyte decreased	3	(12.5)		–
Platelet decreased	1	(4.2)		–
Blood creatine phosphokinase increased	1	(4.2)	1	(4.2)
Leukocyte increased	1	(4.2)		–

MedDRA/J Version 14.0. Event name: the same event name seen in the same patient was counted as one case.

GBM patient and 1 recurrent GBM patient) or IMRT therapy (1 recurrent anaplastic astrocytoma patient), leukocytopenia (grade 2) was noted in a patient who underwent BEV therapy and alopecia (grade 2) and malaise (grade 2) were noted in a patient who underwent IMRT therapy.

III. Pharmacokinetics

BCNU levels in whole blood were measured in 6 of the patients who received BCNU implants. The age of these 6 patients (mean ± SD) was 45.5 ± 15.7 years (21–61 years), body weight was 59.2 ± 14.2 kg (42.9–77.1 kg), median number of BCNU implant sheets inserted was 8 sheets (5–8 sheets: 8 in 4 cases, 7 and 5 in 1 case each), and the administration of BCNU at a median dose level were 61.6 mg (38.5–61.6 mg). As shown in Fig. 6, BCNU levels reached a peak approximately 3 hours after insertion and ranged from 6.49 ng/mL to 19.4 ng/mL (10.19 ± 4.77 ng/mL). After 24 hours, levels were in the vicinity of or below the lower limit of quantification (2.00 ng/mL).

Discussion

This study (NPC-08 study) was designed to evaluate the efficacy, safety, and pharmacokinetics of BCNU implants with chemotherapy (including TMZ) and radiotherapy for Japanese patients with newly diagnosed MGs or recurrent GBM (under conditions indicated for BCNU in USA and Europe). Of the 24 patients who received BCNU implants (newly diagnosed MG, 16 cases; recurrent MG, 8 cases), the survival rate for patients with newly diagnosed MGs was 100.0% at 12 months and 68.8% at 24

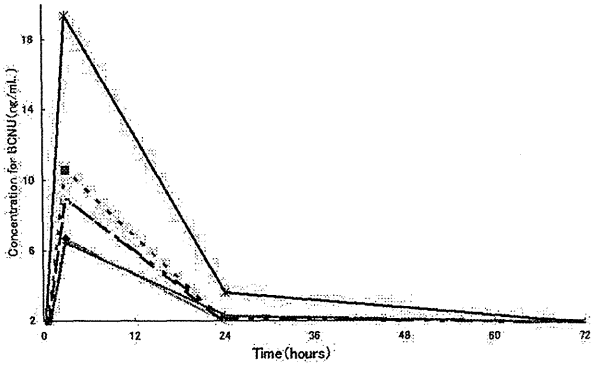

Fig. 6 Time course of BCNU levels in whole blood. Six Japanese patients with malignant gliomas received the maximum blood concentration of BCNU at about 3 hours after implant placement was 19.4 ng/mL. The lower limit of quantitation (2.00 ng/mL).

months, making it impossible to calculate the median survival time in this group. These results were superior those of placebo-controlled double-blind comparative studies[3,4] conducted in USA and Europe in which the OS rate at 12 months was 59.2% (95% CI: 50.4–68.0%) and the mOS was 13.8 months (95% CI: 12.1–15.1 months). However, these studies from USA and Europe were not combined therapy involving TMZ plus radiotherapy for newly diagnosed MGs cases. In NPC-08 study, combined TMZ plus radiotherapy was applied to all patients with newly diagnosed MGs after insertion of BCNU implants. According to previous reports[9–13] examining combined TMZ plus radiotherapy after insertion of BCNU implants, the OS rate at 12 months and 24 months was 56.8–81.0% and 13.0–47.0%. Furthermore, the OS rate at 6 months with recurrent MG was 87.5% in NPC-08 study. According to a clinical study by Brem et al.,[2] the OS rate at 6 months in patients with recurrent MG was 60%. Thus, although the number of patients studied was small, the results of the NPC-08 study were comparable to the results of USA and European studies.

Potential adverse effects of BCNU implants were noted in 13 of 24 patients (54.2%). Severe adverse reactions were noted in 5 of 24 patients (20.8%), although none were live threatening. Important adverse events requiring close attention include brain edema, seizure, poor wound healing, infection, headache, hemiparesis, meningitis, and hydrocephalus according to clinical reports from USA and Europe. We compared the adverse event data in NPC-08 study with the data from three placebo-controlled double-blind comparative studies conducted in USA and Europe (Table 4).

The incidence of Brain edema was higher in the NPC-08 study (25.0%, 6/24 patients) than that in the double-blind studies (4.9%, 12/246 patients). However, there was no significant difference between the BCNU implant group and the placebo group regarding brain edema on grade 3 or worse in the double-blind studies. Brain edema can also be caused by tumor resection, MGs themselves, dose of steroid and so on, therefore, the expression of the brain edema is necessary to be careful, it is necessary to consider the administration of steroid drug. In this study, brain edema of any CTCAE grade occurred in 6 of 24 patients. There were no patients with brain edema of CTCAE grade 4. Two patients developed brain edema of CTCAE grade 3. These two patients were not from a specific facility. We examined the occurrence rate of brain edema by each patient's background in the Japanese studies, but were unable to find any tendency due to the small sample size. Nearly 700 patients were enrolled in foreign studies. Among those patients, 3.8% (26/676) developed brain edema of any CTCAE grade, and 1.9% (12/676) developed brain edema of CTCAE grade 3 or 4. On the other hand, the total number of patients enrolled in the Japanese study was small (24 patients). We consider that this small number of patients (denominator) may have contributed to a large difference; i.e., in the present case, higher rate of brain edema occurrence than in foreign studies. In addition, we infer that one of the reasons that brain edema were more often observed in Japan than in foreign countries is as follows: the protocol for the Japanese study has described "brain edema, convulsion, cerebrospinal fluid (CSF) leakage, and limited hypofunction" as notable adverse events that were reported in foreign studies, and requested investigators and clinical research coordinators to carefully watch for these adverse events. This may have encouraged physicians to conduct CT/MRI testing more frequently than is required in the protocol, leading to observation of higher occurrence rate of brain edema. In summary, although the occurrence rate of brain edema was higher in the Japanese study than in the foreign studies, it is difficult to determine whether the Japanese patients are more likely to develop brain edema than the foreign patients because of the small number of the Japanese patients enrolled in this study. This question should be addressed in future studies. Seizure is one of the complications of brain tumors and neurosurgical interventions, and its incidence differed little between NPC-08 study and the combined double-blind studies. There was no difference between the BCNU implant group and the placebo group in terms of overall incidence or incidence of seizure grade 3 or worse. One of the 3 double-blind studies, Brem et al.[2] reported that the median day of onset of seizures was faster in the BCNU implant group (3.5 days) than in the placebo group (55.5 days) (Wilcoxon test: $P = 0.01$). In the NPC-08 study, the median day of onset of seizures was 91.5 days.

Since the number of patients studied was small, these results were not clear that the day of onset of seizures was tended to be faster by BCNU implant. However, it is necessary to consider the administration of anticonvulsant drugs. None of the patients was experienced poor wound healing after craniotomy as adverse reactions in the NPC-08 study. In the combined double-blind studies, the incidence of poor healing was slightly higher in the BCNU implant group (7.3%, 18/246 patients) than in the placebo group (3.2%, 8/248 patients). Therefore, the expression of poor wound healing is necessary to be careful. Infection and meningitis were not observed

Table 4 Comparison of the number of patients (incidence) who experienced major adverse reactions in the NPC-08 study and in the combined double-blind comparative studies

System organ class/Event name	The NPC-08 study						Double-blind studies[2,10,13]									
	All grades						All grades						Placebo			
	All grades		Grade 3		Grade 4		All grades		Grade 3		Grade 4		All grades		Grade 3		Grade 4	
Total patients	24						246						248					
Brain edema	6	(25.0)	2	(8.3)	–		12	(4.9)	2	(0.8)	3	(1.2)	12	(4.8)	4	(1.6)	2	(0.8)
Seizure		–		–	–		31	(12.6)	7	(2.8)	2	(0.8)	39	(15.7)	11	(4.4)	2	(0.8)
Major seizure		–		–	–		1	(0.4)		–		–	2	(0.8)		–	1	(0.4)
Poor healing		–		–	–		18	(7.3)	4	(1.6)		–	8	(3.2)	1	(0.4)		–
Infection		–		–	–		13	(5.3)	2	(0.8)	3	(1.2)	16	(6.5)	2	(0.8)		–
Headache	2	(8.3)		–	–		28	(11.4)	8	(3.3)		–	22	(8.9)	8	(3.2)	1	(0.4)
Hemiplegia	1	(4.2)		–	–		24	(9.8)	5	(2.0)		–	34	(13.7)	15	(6.0)		–
Monoparesis	1	(4.2)		–	–			–		–		–		–		–		–
Hemiparesis	2	(8.3)	2	(8.3)	–			–		–		–		–		–		–
Meningitis		–		–	–		5	(2.0)	2	(0.8)		–	1	(0.4)		–		–
Hydrocephalus		–		–	–		2	(0.8)	1	(0.4)	1	(0.4)	1	(0.4)		–		–

MedDRA/J Version 14.0. Event name: The same event name seen in the same patient was counted as one case. If severity differed between multiple episodes of the same event, then the most severe episode was selected. Incidence (%) = No. of patients who experienced adverse reaction/all patients studied × 100.

in the NPC-08 study. In the combined double-blind studies, the overall incidence of this event and the incidence of grade 3 or worse differed little between the BCNU implant group and the placebo group, and the incidence was also high in the placebo group.

The incidence of headache was not high in the NPC-08 study (8.3%) and differed little between the BCNU implant group and the placebo group. The incidence of hemiparesis was slightly higher in the combined double-blind studies. Hydrocephalus did not develop in any patient in the NPC-08 study. In the combined double-blind studies, the incidence of hydrocephalus was approximately 0.8% in the BCNU implant group, which was comparable to its incidence in the placebo group. All of the important adverse events discussed above were symptoms accompanying a brain tumor or surgical resection of the tumor.

For pharmacokinetic analysis, BCNU levels in the blood were measured at multiple time points after surgery. The administration of BCNU at a median dose level of 61.6 mg (38.5–61.6 mg) to 6 patients caused a mean peak BCNU level of 10.19 ng/mL. BCNU has been administered intravenously and inserted into the removal cavity for the treatment of brain tumors in USA and Europe. According to a report[14] describing the pharmacokinetics of intravenous BCNU injection, the peak BCNU level in the blood averaged 6.2 μg/mL, whereas the peak level following insertion in the brain averaged 0.01 μg/mL.

Thus, the BCNU level in the blood after insertion into the brain was much lower (1/600) than that after intravenous injection, and BCNU disappears from the blood almost completely within 24 hours of insertion into the brain.

Systemic administration of BCNU often induces severe adverse events such as leucopenia and thrombocytopenia. Insertion of BCNU implants into the brain is expected to markedly reduce systemic adverse events as compared with intravenous BCNU.

Taken together, these results indicate that when insertion of BCNU implants into the brain (maximum of 8 sheets containing a maximum of 61.6 mg BCNU) was followed by chemotherapy or radiotherapy in patients with newly diagnosed or recurrent MGs, there are no major safety concerns associated with the use of BCNU implants. The BCNU implant is now recommended as a treatment option along with the surgical resection of MGs on the basis of established treatment guidelines. The data from this clinical study was comparable to previous data from USA and Europe with respect to efficacy and safety. Therefore, from a risk/benefit viewpoint, the use of BCNU implants is recommended.

Acknowledgments

The authors are indebted to many professionals involved in the NPC-08 study including neurosurgeons; physicians specializing in radiological treatment, chemotherapy, or pathological diagnosis; nurses; pharmacists; clinical trial coordinators; and many others in addition to the 24 patients who participated in the study. The authors greatly appreciate their support. Special thanks to the NPC-08 study group.

Clinical investigators

(a) Saitama Medical University International Medical Center: Kenji Wakiya and Tomonari Suzuki; (b) Kitano Hospital: Hiroki Toda, Jun Takahashi, Tsuyoshi Ota, Namiko Nishida, Hideki Hayashi, Yoshitaka Kurosaki, Koichi Fujimoto, and Taichi Ikedou; (c) Graduate School of Biomedical & Health Sciences, Hiroshima University: Yoshinori Kajiwara, Taiichi Saitou, Yousuke Watanabe, and Takeshi Takayasu; (d) Tohoku University Graduate School of Medicine: Yukihiko Sonoda, Ryuta Saito, Mika Watanabe, and Hisanori Ariga; (e) Dokkyo Medical University Hospital: Yoshifumi Okada, Masahiro Ogino, Kazushige Itoki, Yoshihiro Abe, and Kanae Mochiki; (f) Faculty of Medicine, University of Tsukuba: Akira Matsumura, Shingo Takano, Kei Nakai, and Hiroyoshi Akutsu; (g) Faculty of Medicine, University of Miyazaki Hospital: Kiyotaka Yokogami, Hisao Uehara, Shiro Miyata, Gou Takeishi, Shinitsu Ryu, Toshikatsu Ikeda, Munetomo Futami, and Tetsuaki Sugimoto; (h) Graduate School of Medical and Dental Sciences, Kagoshima University: Sei Sugata, Hajime Yonezawa, Masanao Mori, and Shingo Fujio.

The efficacy and safety evaluation committee

National Cancer Center Hospital: Soichiro Shibui; Saitama Medical University Hospital: Takamitsu Fujimaki; Tokyo Metropolitan Cancer and Infectious diseases Center Komagome Hospital: Katsuyuki Karasawa.

The central pathological evaluation committee

Gunma University: Youichi Nakazato.

BCNU drug level measurement institution

Celerion Inc: Kirk Newland and Kazuko Aoyagi.

The NPC-08 study received partial financial support from the National Institute of Biomedical Innovation within the framework of the Program for Promotion of Orphan Drug/Medical Device Development. The institute provided financial support without intervening in the study.

Nobelpharma Co. Ltd. sponsored the study, providing support for planning the protocol, monitoring, data

management, statistical analysis, and many other activities in the NPC-08 study.

Conflicts of Interest Disclosure

Dr. Tomokazu Aoki is a member of the medical advisory committee of NPC-08 study and received consulting fees from Nobelpharma Co. Ltd. and an honoraria for speaking from Eisai Co. Ltd. Dr. Ryo Nishikawa is a member of the medical advisory committee of NPC-08 study and received consulting fees from Nobelpharma Co. Ltd. Dr. Nishikawa is also a member of the Avaglio study steering committee (funded by F. Hoffmann-La Roche, Ltd) and has received research funding and speaking fees from MSD KK as well as honoraria for speaking from Eisai Co. Ltd. Dr. Kazuhiko Sugiyama is a member of the medical advisory committee of NPC-08 study and received consulting fees from Nobelpharma Co. Ltd. and honoraria for speaking from Eisai Co. Ltd. Dr. Masao Matsutani is a coordinating investigator of NPC-08 study, a member of the advisory committee of MSD KK, and a coordinating investigator for Chugai Pharmaceutical Co. Ltd. Dr. Matsutani also received consulting fees from Nobelpharma Co. Ltd.

The authors declare no other conflicts of interest.

References

1) Committee of Brain Tumor Registry of Japan: Report of brain tumor registry of Japan (1984–2000), *ed 12. Neurol Med Chir (Tokyo)* 49(Suppl): S1–S96, 2009
2) Brem H, Piantadosi S, Burger PC, Walker M, Selker R, Vick NA, Black K, Sisti M, Brem S, Mohr G: Placebo-controlled trial of safety and efficacy of intraoperative controlled delivery by biodegradable polymers of chemotherapy for recurrent gliomas. The Polymer-brain Tumor Treatment Group. *Lancet* 345: 1008–1012, 1995
3) Valtonen S, Timonen U, Toivanen P, Kalimo H, Kivipelto L, Heiskanen O, Unsgaard G, Kuurne T: Interstitial chemotherapy with carmustine-loaded polymers for high-grade gliomas: a randomized double-blind study. *Neurosurgery* 41: 44–48; discussion 48–49, 1997
4) Westphal M, Hilt DC, Bortey E, Delavault P, Olivares R, Warnke PC, Whittle IR, Jääskeläinen J, Ram Z: A phase 3 trial of local chemotherapy with biodegradable carmustine (BCNU) wafers (Gliadel wafers) in patients with primary malignant glioma. *Neuro Oncol* 5: 79–88, 2003
5) National Comprehensive Cancer Network (NCCN) Clinical Practice Guidelines in Oncology-v.1, 2013
6) National Cancer Institute Cancer Information Physician Data Query (May, 2012)
7) National Institute for Health and Clinical Excellence. (June, 2007)
8) Stupp R, Mason WP, van den Bent MJ, Weller M, Fisher B, Taphoorn MJ, Belanger K, Brandes AA, Marosi C, Bogdahn U, Curschmann J, Janzer RC, Ludwin SK, Gorlia T, Allgeier A, Lacombe D, Cairncross JG, Eisenhauer E, Mirimanoff RO; European Organisation for Research and Treatment of Cancer Brain Tumor and Radiotherapy Groups; National Cancer Institute of Canada Clinical Trials Group: Radiotherapy plus concomitant and adjuvant temozolomide for glioblastoma. *N Engl J Med* 352: 987–996, 2005
9) Affronti ML, Heery CR, Herndon JE, Rich JN, Reardon DA, Desjardins A, Vredenburgh JJ, Friedman AH, Bigner DD, Friedman HS: Overall survival of newly diagnosed glioblastoma patients receiving carmustine wafers followed by radiation and concurrent temozolomide plus rotational multiagent chemotherapy. *Cancer* 115: 3501–3511, 2009
10) Bock HC, Puchner MJ, Lohmann F, Schütze M, Koll S, Ketter R, Buchalla R, Rainov N, Kantelhardt SR, Rohde V, Giese A: First-line treatment of malignant glioma with carmustine implants followed by concomitant radiochemotherapy: a multicenter experience. *Neurosurg Rev* 33: 441–449, 2010
11) Larocca RV, Vitaz TW, Morassutti DJ, Doyle MJ, Glisson SD, Hargis JB, Goldsmith GH, Cervera A, Stribinskiene L, New P: A phase II study of radiation with concomitant and then sequential temozolomide (TMZ) in patients with newly diagnosed supratentorial high-grade malignant glioma who have undergone surgery with carmustine (BCNU) wafer insertion. *Neuro Oncol* 8: 391–500, 2006
12) McGirt MJ, Than KD, Weingart JD, Chaichana KL, Attenello FJ, Olivi A, Laterra J, Kleinberg LR, Grossman SA, Brem H, Quiñones-Hinojosa A: Gliadel (BCNU) wafer plus concomitant temozolomide therapy after primary resection of glioblastoma multiforme. *J Neurosurg* 110: 583–588, 2009
13) Pan E, Mitchell SB, Tsai JS: A retrospective study of the safety of BCNU wafers with concurrent temozolomide and radiotherapy and adjuvant temozolomide for newly diagnosed glioblastoma patients. *J Neurooncol* 88: 353–357, 2008
14) Jones RB, Matthes S, Shpall EJ, Fisher JH, Stemmer SM, Dufton C, Stephens JK, Bearman SI: Acute lung injury following treatment with high-dose cyclophosphamide, cisplatin, and carmustine: pharmacodynamic evaluation of carmustine. *J Natl Cancer Inst* 85: 640–647, 1993

Address reprint requests to: Tomokazu Aoki, MD, PhD, Department of Neurosurgery, National Hospital Organization Kyoto Medical Center, 1-1, Fukakusa Mukaibatacho, Fushimi-ku, Kyoto, Kyoto 612-8555, Japan.
e-mail: totorolangdom@yahoo.co.jp

Comparison of Multiple Parameters Obtained on 3T Pulsed Arterial Spin-Labeling, Diffusion Tensor Imaging, and MRS and the Ki-67 Labeling Index in Evaluating Glioma Grading

H. Fudaba, T. Shimomura, T. Abe, H. Matsuta, Y. Momii, K. Sugita, H. Ooba, T. Kamida, T. Hikawa, and M. Fujiki

ABSTRACT

BACKGROUND AND PURPOSE: Pulsed arterial spin-labeling, DTI, and MR spectroscopy provide useful data for tumor evaluation. We evaluated multiple parameters by using these pulse sequences and the Ki-67 labeling index in newly diagnosed supratentorial gliomas.

MATERIALS AND METHODS: All 32 patients, with grade II (3 each of diffuse astrocytoma, oligodendroglioma, and oligoastrocytoma), grade III (3 anaplastic astrocytomas, 4 anaplastic oligodendrogliomas, and 1 anaplastic oligoastrocytoma), and grade IV (14 glioblastomas and 1 glioblastoma with an oligodendroglioma component) cases underwent pulsed arterial spin-labeling, DTI, and MR spectroscopy studies by using 3T MR imaging. The following variables were used to compare the tumors: relative cerebral blood flow, fractional anisotropy; ADC tumor/normal ratios; and the Cho/Cr, NAA/Cho, NAA/Cr, and lactate/Cr ratios. A logistic regression and receiver operating characteristic analysis were used to assess parameters with a high sensitivity and specificity to identify the threshold values for separate grading. We compared the Ki-67 index with various MR imaging parameters in tumor specimens.

RESULTS: Significant correlations were observed between the Ki-67 index and the mean, maximum, and minimum ADC, Cho/Cr, and lactate/Cr ratios. The receiver operating characteristic analysis showed that the combination of the minimum ADC and Cho/Cr ratios could differentiate low-grade and high-grade gliomas, with a sensitivity and specificity of 87.0% and 88.9%, respectively. The mean and maximum relative cerebral blood flow ratios were used to classify glioblastomas from other-grade astrocytomas, with a sensitivity and specificity of 92.9% and 83.3%, respectively.

CONCLUSIONS: Our findings indicate that pulsed arterial spin-labeling, DTI, and MR spectroscopy are useful for predicting glioma grade. Additionally, the parameters obtained on DTI and MR spectroscopy closely correlated with the proliferative potential of gliomas.

ABBREVIATIONS: ASL = arterial spin-labeling; C1 error = average observed sensitivity and specificity; C2 error = observed number of instances of tumor-grade misclassification; FA = fractional anisotropy; Lac = lactate; NPV = negative predictive value; PASL = pulsed arterial spin-labeling; PPV = positive predictive value; rCBF = relative cerebral blood flow; ROC = receiver operating characteristic

Grading gliomas is necessary to determine the appropriate treatment strategy and assess prognosis. Classifying lesions into 4 grades based on histologic analyses requires tumor specimens obtained via biopsy or surgical resection.[1]

On conventional MR imaging with gadolinium contrast, the presence of FLAIR abnormalities or gadolinium enhancement reveals the appearance of new lesions. Advanced MR imaging, pulsed arterial spin-labeling (PASL), DTI, and MR spectroscopy provide useful data for evaluating tumors preoperatively. The PASL technique allows cerebral blood flow to be measured noninvasively without exogenous contrast agents. The usefulness of perfusion MR imaging with arterial spin-labeling (ASL) for assessing brain tumor angiogenesis and grading gliomas has been evaluated.[2-7] DTI provides information on anisotropy, including fractional anisotropy (FA), and ADC. A recent study investigating DTI of gliomas showed that the FA and ADC tumor/normal tissue ratios are possible indicators of glioma proliferation and/or grading.[8-10] MR spectroscopy is also a noninvasive method that allows the measurement of various metabolites in vivo, such as Cho, Cr, NAA, and the pathologic levels of lactate (Lac), and has been reported useful for investigating gliomas.[11-13] The use of a combination of these noninvasive parameters has been reported to increase the diagnostic accuracy of glioma grading.[7,9,11,12,14-18]

Received February 20, 2014; accepted after revision April 25.

From the Department of Neurosurgery, Oita University Faculty of Medicine, Oita, Japan.

This work was supported by a grant from the Japan Science and Technology Agency and the Ministry of Education, Culture, Sports, Science and Technology.

Please address correspondence to Hirotaka Fudaba, MD, Department of Neurosurgery, Oita University Faculty of Medicine, Oita, 879-5593 Japan; e-mail: fudaba@oita-u.ac.jp

Indicates open access to non-subscribers at www.ajnr.org

Indicates article with supplemental on-line table.

http://dx.doi.org/10.3174/ajnr.A4018

Very few reports describe comparisons of multiple parameters, including the relative cerebral blood flow (rCBF)-measured PASL sequence on 3T MR imaging, and glioma grading. Immunohistologically, the Ki-67 labeling index on histologic examinations is known to correlate with malignancy, and it also functions as a marker of proliferation in gliomas.[19] According to the previous literature, this index is correlated with various advanced MR imaging parameters.[8,20,21]

In this study, we performed a comparative review of multiple parameters obtained with pulse sequences evaluated by using 3T MR imaging and glioma grading in newly diagnosed patients with glioma. Our purpose was to evaluate whether the parameters provide useful, complementary information and whether this combination of parameters shows the best performance for grading cerebral gliomas. The results of the present study are clinically valuable for evaluating sensitivity, specificity, positive predictive value (PPV), and negative predictive value (NPV) and determining the threshold values by analyzing receiver operating characteristic (ROC) curves. Under the same conditions, we evaluated the correlations between various MR imaging parameters and the proliferation marker, the Ki-67 labeling index.

MATERIALS AND METHODS

Patients

Thirty-two patients ranging in age from 16 to 82 years with newly diagnosed supratentorial glioma, to avoid confounding findings related to posttherapeutic effects, were entered into this study. All patients underwent PASL, DTI, and MR spectroscopy studies by using 3T MR imaging. We reviewed all PASL, FA, ADC, and MR spectroscopy studies of supratentorial cerebral gliomas performed between March 2010 and October 2012. No patients had a clinical history of previous surgery, chemotherapy, or radiation therapy.

The histologic analysis was performed, according to the World Health Organization brain tumor classification revised in 2007, of tissue samples obtained at the time of either surgical resection or image-guided biopsies.[1]

All patients provided their informed consent to participate in this study, which was conducted in accordance with the ethical principles of the Declaration of Helsinki. The study protocol was approved by the Ethics Committee of the Oita University Faculty of Medicine.

MR Imaging Protocol

Conventional MR imaging included T1-weighted spin-echo, T2-weighted fast spin-echo, fluid-attenuated inversion recovery, and contrast-enhanced T1-weighted axial imaging (0.1-mmol/kg meglumine gadoterate, Magnescope; Guerbet Japan, Tokyo, Japan) performed at a field strength of 1.5T. After 2–5 days, we performed the advanced MR imaging examination. All participating patients underwent an advanced MR imaging protocol that included PASL, DTI, MR spectroscopy, and SWI by using a superconducting magnet at a field strength of 3T (Magnetom Verio; Siemens, Erlangen, Germany). T1-weighted structural images were acquired with a 3D MPRAGE device in the sagittal plane. The imaging parameters were as follows: TR/TE = 1900/2.53 ms, TI = 900 ms, flip angle = 9°, FOV = 21.0 cm, section thickness = 1 mm, section gap = 0.5 mm, number of sections collected = 176, matrix = 192 × 192 × 256. An SWI sequence was performed to detect calcification and hemorrhagic areas. On the basis of advanced MR imaging, rCBF, FA, ADC, and MR spectra were calculated by the MR imaging console software program (syngo MR B17; Siemens).

Pulsed Arterial Spin-Labeling

We performed pulsed arterial spin-labeling perfusion MR imaging by using QUIPSS II with thin-slice TI1 periodic saturation (Q2TIPS).[22] The Q2TIPS technique is a pulsed arterial spin-labeling method that enables the acquisition of multiple sections. The inversion and saturation pulse parameters of Q2TIPS were set as follows: TI1 = 700 ms, TI1S = 1600 ms, and TI2 = 1800 ms. The other imaging parameters were as follows: TR/TE = 2800/13 ms, flip angle = 90°, FOV = 25.6 cm, section thickness = 8 mm, voxel size = 4 × 4 × 8 mm, section number = 9. Crusher gradients were not used. The total acquisition time was 4 minutes 19 seconds. Motion correction was interpolated according to the 3D *k*-space method, with a spatial filter setting of 2.0.

Diffusion Tensor Imaging

Axial DTI was performed by using single-shot spin-echo echo-planar imaging sequences. The parameters were as follows: TR/TE = 9200/96 ms, FOV = 23.0 cm, matrix = 128 × 128, b=0 s/mm^2 as reference imaging and b=1000 s/mm^2, diffusion-sensitive dimensions = 12, average = 3, scanning time = 6 minutes 28 seconds.

PASL and Diffusion Tensor Images

After reconstruction, the PASL, FA, and ADC images were converted into the DICOM format and inserted into the data base. To minimize confounding factors in the analysis, we kept the size of the ROIs in the lesion and contralateral normal brain constant (diameter = 8.0 mm) on both the PASL and diffusion tensor images. Two observers placed 5 ROIs each within the solid tumor component and 1 region of interest each in the contralateral normal brain.[6] Whenever possible, the ROIs were placed in mirrored white matter regions; when this placement was not possible, the ROIs were positioned in representative normal white matter in the same transaxial plane.[14] Care was taken to ensure that the ROIs were entirely within the solid part of the lesion to avoid contamination of the region of interest from normal tissue, areas of necrosis, cysts, hemorrhage, or intratumoral mineralization. We placed the ROIs at the site of the enhanced lesions on the contrast-enhanced T1-weighted MR images. In patients with nonenhancing tumors, the tumor parenchyma was identified as the area of hyperintensity on T2-weighted and FLAIR images. The ROIs were evaluated for eligibility independently by 2 authors (H.F. and T.S.), and any disagreements were resolved by consensus.

The rCBF, FA, and ADC ratios were calculated as follows: rCBF (FA or ADC) ratio = rCBF (FA or ADC) [tumor] / rCBF (FA or ADC) [contralateral normal tissue]. The average values of the minimum, maximum, and mean of the rCBF, FA, and ADC ratios were then selected for the analysis.

MR Spectroscopy

A single-voxel water-suppressed point-resolved spectroscopy sequence and multivoxel chemical shift imaging were performed. The single-voxel water-suppressed point-resolved spectroscopy sequence was performed by using the following parameters: TR/TE = 2000/270 ms, flip angle = 90°, voxel size = 20 × 20 × 20 mm (normal-sized lesion) or 15 × 15 × 15 mm (small lesion: lesions measuring less than approximately 20 mm in diameter), acquisition average = 192 (normal-sized lesion) or 256 (small lesion). The total acquisition time was 6 minutes 32 seconds (normal-sized lesion) or 8 minutes 40 seconds (small lesion). Multivoxel chemical shift imaging was performed by using the following parameters: TR/TE = 1700/270 ms, flip angle = 90°, FOV = 16.0 cm, section thickness = 8 mm, voxel size = 10 × 10 × 8 mm, acquisition average = 5. The total acquisition time was 9 minutes 26 seconds. The single-voxel water-suppressed point-resolved spectroscopy sequence was primarily performed; however, multivoxel chemical shift imaging was performed in cases of deep and centrally located tumors measuring >3 cm in diameter because for some temporal lobe and inferior frontal lobe tumors, adequate shimming can be problematic, while for intraventricular tumors and/or very peripheral tumors, CSF or scalp fat contamination may adversely affect MR spectroscopy acquisition. We selected the region of interest of the multivoxel area in the center region to prevent the influence of magnetic susceptibility and to optimize the shimming procedure. To the extent possible, we selected the multivoxel technique because the previous literature suggests that multivoxel MR spectroscopy is more useful for distinguishing glioma recurrence from posttreatment effects than single-voxel MR spectroscopy.[23]

The spectra were automatically analyzed for the relative signal intensity (area under the fitted peaks in the time domain) of the following metabolites: Cho, Cr, NAA, and Lac. The ratios of Cho/Cr, NAA/Cho, NAA/Cr, and Lac/Cr at TE 270 ms were calculated. The postprocessing steps, including the frequency shift, baseline correction, phase correction, and peak fitting/analysis, were performed first automatically and then manually. All spectral analyses were conducted within a window from 0.50 to 4.30 ppm (by using the standard method of assigning a shift value of 4.7 ppm to the measured unsuppressed water peak). The metabolite peak areas were assigned as follows: Cho, 3.20 ppm; Cr, 3.02 ppm; NAA, 2.00 ppm; Lac, 1.29 ppm. To avoid contamination of the voxel from normal tissue or areas of necrosis or cysts based on conventional MR imaging, we obtained the metabolite ratios within the solid portion of the lesion by consensus without knowledge of the final histologic tumor diagnosis.

Immunohistologic Assay

For Ki-67 immunostaining, the specimens were sliced from formalin-fixed, paraffin-embedded tissues. We stained the sections with a mouse anti-Ki-67 monoclonal antibody (MIB-1; Dako Cytomation, Carpinteria, California; 1:50 dilution). The Ki-67 labeling index, defined as the number of positive tumor cells / the total number of tumor cells × 100%, was calculated for at least 10 fields selected at random under a magnification ×400.

Statistical Analysis

We compared the MR imaging parameters and the Ki-67 labeling index in each of 3 groups (grade II versus grade III versus grade IV) by using the Tukey-Kramer test. The sensitivity, specificity, PPV, and NPV were calculated by using an ROC analysis to correctly identify high-grade gliomas (grade III and IV) and glioblastomas (grade IV), to differentiate the 2 groups, such as patients with high- and low-grade gliomas and those with glioblastomas and other-grade gliomas (grade II and III). Because oligodendroglial tumors tend to demonstrate hyperperfusion relative to astrocytic tumors, we also analyzed the CBF data only for purely astrocytic tumors that did not contain oligodendroglial regions, such as diffuse astrocytomas, anaplastic astrocytomas, and glioblastomas. The optimal threshold values were those that did the following: 1) minimized the observed number of instances of tumor-grade misclassification (C2 error = fraction of misclassified tumors), and 2) maximized the average observed sensitivity and specificity (C1 error) resulting in C1 = 1 − (sensitivity + specificity) / 2. To determine the combination of the most discriminative parameters, we used a stepwise multiple logistic backwards regression. The logistic regression was selected by using a cutoff level of .05 for significance. The correlations between the MR imaging parameters and the Ki-67 labeling index were analyzed statistically by using a Spearman correlation coefficient analysis.

RESULTS

Among 32 patients, 9 tumors were grade II (3 each of diffuse astrocytoma, oligodendroglioma, and oligoastrocytoma), 8 tumors grade III (3 anaplastic astrocytomas, 4 anaplastic oligodendrogliomas, and 1 anaplastic oligoastrocytoma), and 15 tumors grade IV (14 glioblastomas and 1 glioblastoma with an oligodendroglioma component). The patients included 13 men and 19 women, with a mean age of 59.8 ± 16.8 years. The conventional MR imaging characteristics of the tumors are shown in the Online Table. Patient 27 was unable to undergo an examination by using contrast agent due to her current treatment with dialysis. We performed multivoxel MR spectroscopy in 9 cases and single-voxel MR spectroscopy in 23 cases. Examples of low-grade and high-grade glial neoplasms are provided in Figs 1 and 2, respectively.

Both the mean ADC ratio ($r = -0.455$, $P = .0113$) and maximum ADC ratio ($r = -0.352$, $P = .0497$) exhibited a negative correlation with the Ki-67 index. In particular, there was a significant negative correlation between the minimum ADC ratio and the Ki-67 index ($r = -0.470$, $P = .0089$). A positive correlation was also observed between the Cho/Cr ratio and the Ki-67 index ($r = 0.461$, $P = .0103$) and between the Lac/Cr ratio and the Ki-67 index ($r = 0.418$, $P = .0199$). In contrast, no significant correlations were noted between the other parameters and the Ki-67 index.

The maximum rCBF ratio of the grade IV gliomas was higher than that of the grade III gliomas, while the Ki-67 labeling index of the grade II gliomas was lower than that of the grade III and grade IV gliomas ($P < .05$). The maximum FA ratio associated with grade II gliomas was lower than that associated with the grade IV gliomas, while the mean and minimum ADC ratios of grade II gliomas were higher than those of grade IV gliomas ($P < .05$).

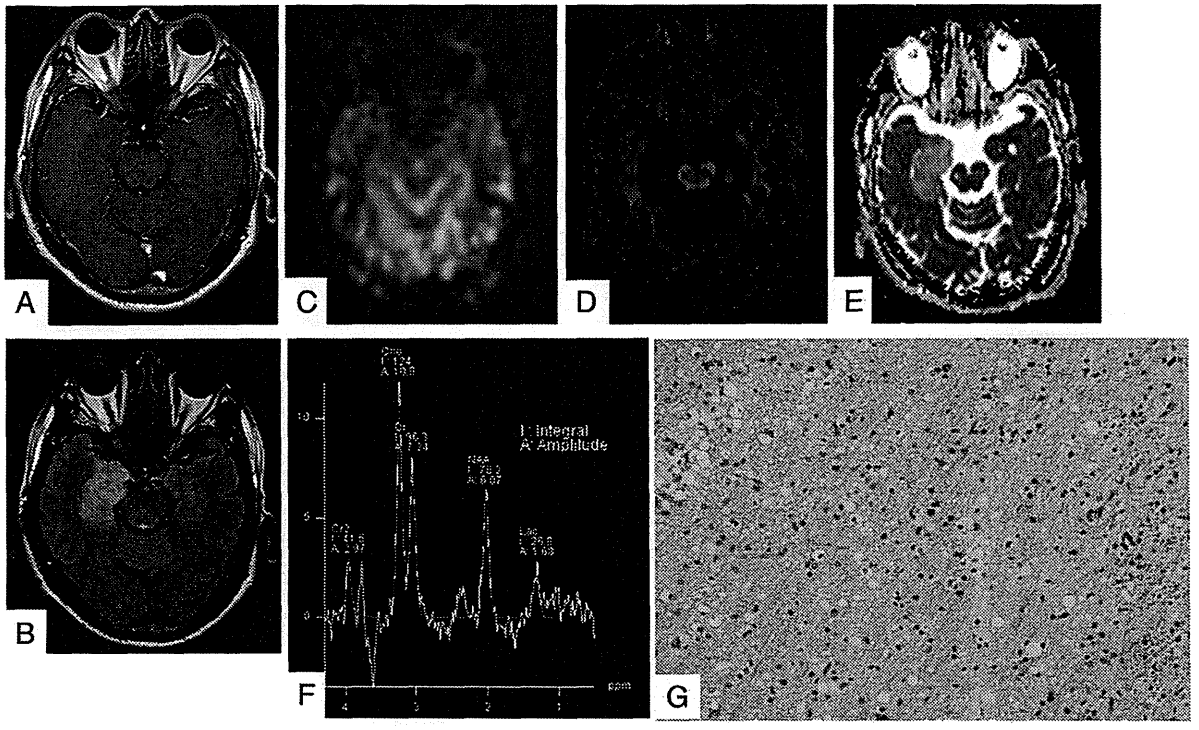

FIG 1. A 62-year-old man with a grade II oligoastrocytoma. The contrast-enhanced T1-weighted image shows a nonenhancing mass in the right hippocampus (*A*). The lesions presented high-intensity signals on FLAIR images (*B*). The rCBF map on PASL shows no areas of hyperperfusion (*C*). The FA map shows low FA values (*D*). The ADC map shows increased tumor diffusion values (*E*). The tumor MR spectrum shows decreased NAA and slightly increased Cho and Lac (*F*). The Ki-67 labeling index is 5.0% (original magnification × 400) (*G*).

Other comparisons did not reveal any statistically significant differences.

Regarding the parameters calculated from PASL, DTI, and MR spectroscopy, the threshold values were obtained separately for the minimum C1 and C2 errors, as shown in Tables 1 and 2. With respect to individual parameters for separating high-grade from low-grade gliomas, a threshold value of 1.789 for the Lac/Cr ratio, which exhibited the best performance for a minimum C1 error, provided sensitivity, specificity, PPV, and NPV of 73.9%, 100.0%, 100.0%, and 60.0%, respectively. Meanwhile, a threshold value of 1.789 for the Cho/Cr ratio, which exhibited the best performance for a minimum C2 error, provided sensitivity, specificity, PPV, and NPV of 91.3%, 77.8%, 91.3%, and 77.8%, respectively. Regarding individual parameters for separating glioblastomas from other-grade gliomas, a threshold value of 2.845 for the maximum rCBF ratio, which exhibited the best performance for minimum C1 and C2 errors, provided sensitivity, specificity, PPV, and NPV of 86.7%, 82.4%, 81.3%, and 87.5%, respectively. In particular, for evaluating purely astrocytic tumors, both the mean and maximum rCBF ratios demonstrated sensitivity, specificity, PPV, and NPV of 92.9%, 83.3%, 92.8%, and 83.4%, respectively.

According to multivariate logistic regression analysis, the combinations of parameters for differentiating high- and low-grade gliomas included the minimum ADC and Cho/Cr ratios, while those for differentiating glioblastomas and other-grade gliomas included the maximum rCBF and mean ADC ratios. The results of the ROC analyses by using these combinations are shown in Tables 3 and 4. The combination of the minimum ADC ratio and the Cho/Cr ratio provided sensitivity, specificity, PPV, and NPV of 87.0%, 88.9%, 95.2%, and 72.7%, respectively, for minimum C1 and C2 errors for differentiating high- and low-grade gliomas. Meanwhile, the combination of the maximum rCBF ratio and the mean ADC ratio provided sensitivity, specificity, PPV, and NPV of 73.3%, 94.1%, 91.7%, and 80.0%, respectively, for minimum C1 and C2 errors for differentiating glioblastomas and other-grade gliomas. This combination appears to be inferior compared with the minimum C1 and C2 errors of the maximum rCBF ratio; however, its accuracy was 84.4%, which is as high as that observed for the maximum rCBF ratio.

DISCUSSION

Cerebral gliomas are important and the most common primary brain tumors. MR imaging plays a critical role in the preoperative assessment and grading of gliomas. The classification and grading of gliomas on conventional MR imaging are sometimes unreliable. The sensitivity, specificity, PPV, and NPV for identifying high-grade gliomas on conventional MR imaging are 72.5%, 65.0%, 86.1%, and 44.1%, respectively.[15] The current study demonstrated contrast enhancement in 66.7%, 75.0%, and 100% of grade II, III, and IV gliomas, respectively, which suggests that it is difficult to perform glioma grading by only using structural gadolinium-enhanced MR imaging.[17] Physicians must perform a biopsy or surgical resection to make a pathologic diagnosis and evaluate the need for postoperative chemoradiotherapy. However, lesions for which the risks of biopsy are high cannot be accurately diagnosed and graded. The noninvasive evaluation of

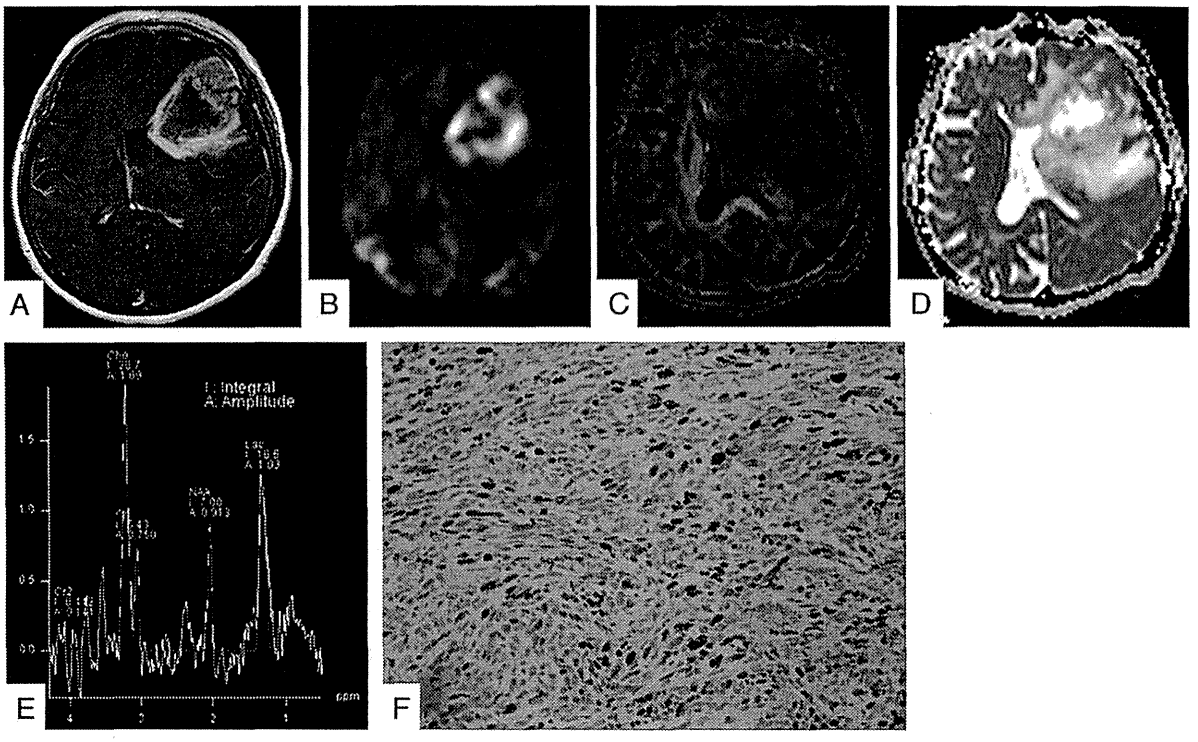

FIG 2. A 60-year-old woman with a grade IV glioblastoma. The lesion on the left frontotemporal lobe exhibits strong enhancement on gadolinium T1-weighted image (*A*). The neoplasm is clearly hyperperfused compared with the healthy parenchyma on the PASL image (*B*). The FA map shows slightly low FA values (*C*). The ADC map shows heterogeneous tumor diffusion values (*D*). The tumor MR spectrum shows decreased NAA with a marked increase in Cho and Lac (*E*). The Ki-67 labeling index is 27.0% (original magnification × 400) (*F*).

Table 1: Threshold values for multiple parameters for differentiating high- and low-grade gliomas

	Based on Minimum C1 Error					Errors		Based on Minimum C2 Error					Errors	
Parameters	Threshold	Sensitivity	Specificity	PPV	NPV	C1	C2	Threshold	Sensitivity	Specificity	PPV	NPV	C1	C2
rCBF ratio mean	2.562	0.652	0.778	0.882	0.467	0.285	0.170	2.562	0.652	0.778	0.882	0.467	0.285	0.170
rCBF ratio max	2.845	0.609	0.778	0.875	0.438	0.307	0.202	2.845	0.609	0.778	0.875	0.438	0.307	0.202
rCBF ratio min	2.017	0.739	0.667	0.850	0.500	0.297	0.179	2.017	0.739	0.667	0.850	0.500	0.297	0.179
rCBF ratio mean[a]	1.800	0.824	0.667	0.933	0.401	0.255	0.142	1.800	0.824	0.667	0.933	0.401	0.255	0.142
rCBF ratio max[a]	2.258	0.765	0.667	0.929	0.334	0.284	0.166	2.258	0.765	0.667	0.929	0.334	0.284	0.166
rCBF ratio min[a]	1.254	0.882	0.667	0.938	0.499	0.226	0.125	1.254	0.882	0.667	0.938	0.499	0.226	0.125
FA ratio mean	0.236	0.870	0.556	0.834	0.626	0.287	0.214	0.267	0.739	0.667	0.850	0.500	0.297	0.179
FA ratio max	0.288	0.870	0.667	0.870	0.668	0.232	0.128	0.288	0.870	0.667	0.870	0.668	0.232	0.128
FA ratio min	0.279	0.565	0.667	0.813	0.375	0.384	0.300	0.279	0.565	0.667	0.813	0.375	0.384	0.300
ADC ratio mean	1.659	0.913	0.667	0.875	0.750	0.210	0.118	1.659	0.913	0.667	0.875	0.750	0.210	0.118
ADC ratio max	1.538	0.826	0.556	0.826	0.556	0.309	0.227	1.538	0.826	0.556	0.826	0.556	0.309	0.227
ADC ratio min	1.564	0.913	0.667	0.875	0.750	0.210	0.118	1.564	0.913	0.667	0.875	0.750	0.210	0.118
Cho/Cr	1.789	0.913	0.778	0.913	0.778	0.155	0.057	1.789	0.913	0.778	0.913	0.778	0.155	0.057
NAA/Cho	0.349	0.696	0.778	0.889	0.500	0.263	0.142	0.349	0.696	0.778	0.889	0.500	0.263	0.142
NAA/Cr	1.289	0.304	1.000	1.000	0.360	0.348	0.484	0.894	0.478	0.778	0.846	0.368	0.372	0.322
Lac/Cr	1.789	0.739	1.000	1.000	0.600	0.131	0.068	1.789	0.739	1.000	1.000	0.600	0.131	0.068

Note:—min indicates minimum; max, maximum.

[a] rCBF ratios derived from purely astrocytomas.

gliomas results in a more precise assessment for selecting the surgical approach or chemoradiotherapy.

In the present study, the combination of the minimum ADC ratio and the Cho/Cr ratio exhibited a high sensitivity and specificity for distinguishing high- and low-grade gliomas. The mean ADC and minimal ADC values have been reported to be correlated with the tumor cell attenuation and thus used to grade astrocytomas.[10,14] In addition, the ADC ratio has been reported to be useful for grading gliomas.[18] Past studies have revealed that the Cho/Cr ratio tends to increase as glioma malignancy progresses.[13,18] Furthermore, Server et al[18] reported a minimum ADC ratio threshold value of 1.41 and a Cho/Cr threshold value of 1.35 for dividing high- and low-grade gliomas, similar to the results of our analysis. Published data regarding intracranial tumors indicate that a high ADC is attributable to a low level of cellularity, necrosis, or cysts, while a lower ADC is attributable to the presence of an attenuated, highly cellular tumor. The typical spectrum corresponding to a tumor shows an increased Cho peak, which corresponds to increased cell attenuation and membrane turnover in neoplastic tissue. With respect to glioma grading, our results consistently reflect the mitotic activity and presence of microvascular proliferation.

Table 2: Threshold values for multiple parameters for differentiating glioblastomas and other-grade gliomas

	Based on Minimum C1 Error					Errors		Based on Minimum C2 Error					Errors	
Parameters	Threshold	Sensitivity	Specificity	PPV	NPV	C1	C2	Threshold	Sensitivity	Specificity	PPV	NPV	C1	C2
rCBF ratio mean	2.562	0.867	0.765	0.765	0.867	0.184	0.073	2.562	0.867	0.765	0.765	0.867	0.184	0.073
rCBF ratio max	2.845	0.867	0.824	0.813	0.875	0.155	0.049	2.845	0.867	0.824	0.813	0.875	0.155	0.049
rCBF ratio min	2.017	0.867	0.588	0.650	0.834	0.273	0.187	2.164	0.800	0.647	0.667	0.786	0.277	0.165
rCBF ratio mean[a]	1.857	0.929	0.833	0.928	0.834	0.119	0.033	1.857	0.929	0.833	0.928	0.834	0.119	0.033
rCBF ratio max[a]	2.258	0.929	0.833	0.928	0.834	0.119	0.033	2.258	0.929	0.833	0.928	0.834	0.119	0.033
rCBF ratio min[a]	2.164	0.786	0.833	0.917	0.625	0.191	0.074	2.164	0.786	0.833	0.917	0.625	0.191	0.074
FA ratio mean	0.380	0.733	0.765	0.733	0.765	0.251	0.127	0.380	0.733	0.765	0.733	0.765	0.251	0.127
FA ratio max	0.371	0.800	0.588	0.631	0.769	0.306	0.210	0.418	0.667	0.706	0.667	0.706	0.314	0.197
FA ratio min	0.333	0.600	0.647	0.600	0.647	0.377	0.285	0.333	0.600	0.647	0.600	0.647	0.377	0.285
ADC ratio mean	1.305	0.800	0.765	0.750	0.813	0.218	0.095	1.305	0.800	0.765	0.750	0.813	0.218	0.095
ADC ratio max	1.494	0.933	0.529	0.636	0.899	0.269	0.226	1.494	0.933	0.529	0.636	0.899	0.269	0.226
ADC ratio min	1.449	0.933	0.647	0.700	0.916	0.210	0.129	1.148	0.733	0.824	0.786	0.778	0.222	0.102
Cho/Cr	1.789	0.933	0.471	0.609	0.888	0.298	0.284	2.813	0.733	0.647	0.647	0.733	0.310	0.196
NAA/Cho	0.338	0.733	0.647	0.647	0.733	0.310	0.196	0.338	0.733	0.647	0.647	0.733	0.310	0.196
NAA/Cr	1.922	0.200	1.000	1.000	0.586	0.400	0.640	0.725	0.600	0.412	0.474	0.539	0.494	0.506
Lac/Cr	2.778	0.667	0.882	0.833	0.750	0.226	0.125	2.778	0.667	0.882	0.833	0.750	0.226	0.125

[a] rCBF ratio derived from purely astrocytomas.

Table 3: Combination of the minimum ADC ratio and Cho/Cr for differentiating high- and low-grade gliomas

Based on Minimum C1 Error				Errors		Based on Minimum C2 Error				Errors	
Sensitivity	Specificity	PPV	NPV	C1	C2	Sensitivity	Specificity	PPV	NPV	C1	C2
0.870	0.889	0.952	0.727	0.121	0.029	0.870	0.889	0.952	0.727	0.121	0.029

Table 4: Combination of the maximum rCBF ratio and mean ADC ratio for differentiating glioblastomas and other-grade gliomas

Based on Minimum C1 Error				Errors		Based on Minimum C2 Error				Errors	
Sensitivity	Specificity	PPV	NPV	C1	C2	Sensitivity	Specificity	PPV	NPV	C1	C2
0.733	0.941	0.917	0.800	0.163	0.075	0.733	0.941	0.917	0.800	0.163	0.075

On the other hand, the maximum rCBF ratio, in addition to being helpful in combination with the mean ADC ratio, is most useful for differentiating glioblastomas and other-grade gliomas. The minimum ADC ratio was excluded in the logistic analysis, though the minimum ADC ratio of the glioblastomas was significantly lower than that of the other-grade lesions ($P < .05$). Perhaps, this is due to the inclusion of oligodendroglial tumors and astrocytic tumors in the assessment. It is surprising that the parameters obtained on MR spectroscopy did not demonstrate a high utility in differentiating glioblastomas from the remaining tumors. In particular, we did not expect that the sensitivity and specificity of the NAA/Cho ratio would be so low because prior studies have suggested that a prominent elevation of the Cho/NAA ratio is a hallmark of glioblastomas.[13,24] In the present study, we only evaluated astrocytomas, except for oligodendroglial tumors, and found that the maximum and mean rCBF ratios can be used to discriminate glioblastomas and other lesions, with C1 and C2 errors of 11.9% and 3.3%, respectively. Perfusion MR imaging is one of the most effective noninvasive methods for quantifying the grade of neoplastic neovascularization.[5,25-29] Furthermore, neovascularization is one of the most important criteria of malignancy for glioma grading. There has been extensive perfusion research related to predicting the glioma grade, much of it by using the DSC MR imaging technique.[27,28] On the other hand, ASL is a promising tool for assessing tumor angiogenesis and glioma grading.[2-7,26,29] ASL has several advantages, including being a nonionizing and completely noninvasive MR imaging technique that uses magnetically labeled arterial blood water protons as an endogenous tracer. For this reason, ASL is very suitable for diagnosing individuals with renal insufficiency and providing repeat follow-up.

Histologically, glioblastomas statistically have a larger microvessel attenuation than grade III lesions.[30] Previous studies have reported a positive correlation between rCBF-derived continuous ASL and vascular attenuation in gliomas.[3,5] Weber et al[16] attempted to elucidate the relationships between the rCBF on PASL and histopathologic findings, including the cell proliferation index and vessel attenuation, as defined by the number of microvessels. Our results indicated a high level of vascularity in glioblastomas and suggest that rCBF is a potential indicator of malignancy in gliomas based on vascular attenuation.

A multiparametric MR imaging approach has been attempted in past reports. Roy et al[17] studied 56 patients by using conventional MR imaging, DTI, dynamic contrast-enhanced perfusion imaging, and volumetric whole-brain MR spectroscopy and concluded that relative cerebral blood volume can be used to individually classify gliomas as low- or high-grade, with a sensitivity and specificity of 100% and 88%, respectively. On combining this parameter with the maximum relative cerebral blood volume, FA, ADC, and minimal NAA + Cr, classification was achieved with a 2% error and a sensitivity and specificity of 100% and 96%, respectively.[17] Unfortunately, the findings of the present study do not reach these levels of sensitivity and specificity; however, we used the ASL technique, which can measure the rCBF without a contrast agent. Weber et al[16] investigated the functional MR imaging methods DSC and PASL, dynamic contrast-enhanced MR imaging, and MR spectroscopy at 1.5T and suggested that the rCBF derived by using the PASL technique offers superior diagnostic performance in predicting the grade of gliomas. In another study of 1.5T, the combination of PASL and ADC significantly improved the sensitivity and predictive value of the preoperative

grading of gliomas compared with conventional imaging.[4] Only 1 study of the multiparametric MR imaging technique in combination with the ASL perfusion technique at 3T has been reported. Chawla et al[7] showed that the rCBF evaluated by using continuous ASL cannot be used to differentiate low-grade from high-grade gliomas, though the rCBF-guided voxel assessed by using a voxel analysis of multivoxel MR spectroscopy is useful for grading such tumors.

Histologically, we examined the Ki-67 labeling index as a marker of proliferation. Previous studies have shown that a higher rate of Ki-67-positive cells corresponds to greater malignancy and a worse survival rate in patients with gliomas.[19] Our studies demonstrated that the Ki-67 labeling index is correlated with MR imaging parameters, such as the ADC ratio, Cho/Cr ratio, and Lac/Cr ratio, consistent with the findings of previous literature.[20,21,31] These noninvasive imaging modalities can be used to reliably assess the potential for proliferation among brain tumors without a surgical procedure.

This study has several limitations. For example, the design included a relatively small population. In addition, when using diagnostic methods based on histologic biopsies, sampling bias should be considered. Although we used the same size region of interest for the multiple parameters of PASL, FA, and ADC, the region-of-interest diameter was relatively larger than that used in past reports and the effects of tumoral heterogeneity and regional differences were difficult to assess. Our method is based on the findings of an article by Hirai et al[6]; however, the placement of 5 ROIs on the ipsilesional side with only 1 region of interest on the contralateral side appears to be problematic for determining the ideal ratio. Regarding the limitation of the PASL sequence, a section thickness of 8 mm is relatively thick compared with that used in previous literature. We carefully placed the region of interest and minimized the potential for such errors. In the present study, we evaluated the data obtained by using both single-voxel and multivoxel techniques to secure the patients, though there may be a potential weaknesses in analyzing the combined single- and multivoxel MR spectroscopy data. Furthermore, the same TE conditions were used in each MR spectroscopy study to reduce the potential for error.

CONCLUSIONS

Our findings indicate that PASL, DTI, and MR spectroscopy provide useful parameters for predicting malignant grades of cerebral gliomas. In particular, the rCBF ratio calculated by using PASL at a high field strength is useful for distinguishing glioblastomas from grade II or III gliomas. The ADC, Cho/Cr, and Lac/Cr ratios have the potential to predict glioma proliferation.

REFERENCES

1. Louis DN, Ohgaki H, Wiestler OD, et al. **The 2007 WHO classification of tumours of the central nervous system.** *Acta Neuropathol* 2007;114:97–109
2. Warmuth C, Gunther M, Zimmer C. **Quantification of blood flow in brain tumors: comparison of arterial spin labeling and dynamic susceptibility weighted contrast-enhanced MR imaging.** *Radiology* 2003;228:523–32
3. Kimura H, Takeuchi H, Koshimoto Y, et al. **Perfusion imaging of meningioma by using continuous arterial spin-labeling: comparison with dynamic susceptibility-weighted contrast-enhanced MR images and histopathologic features.** *AJNR Am J Neuroradiol* 2006;27:85–93
4. Kim HS, Kim SY. **A prospective study on the added value of pulsed arterial spin-labeling and apparent diffusion coefficients in the grading of gliomas.** *AJNR Am J Neuroradiol* 2007;28:1693–99
5. Noguchi T, Yoshiura T, Hiwatashi A, et al. **Perfusion imaging of brain tumors using arterial spin-labeling: correlation with histopathologic vascular density.** *AJNR Am J Neuroradiol* 2008;29:688–93
6. Hirai T, Kitajima M, Nakamura H, et al. **Quantitative blood flow measurements in gliomas using arterial spin-labeling at 3T: intermodality agreement and inter- and intraobserver reproducibility study.** *AJNR Am J Neuroradiol* 2011;32:2073–79
7. Chawla S, Wang S, Wolf RL, et al. **Arterial spin-labeling and MR spectroscopy in the differentiation of gliomas.** *AJNR Am J Neuroradiol* 2007;28:1683–89
8. Zikou AK, Alexiou GA, Kosta P, et al. **Diffusion tensor and dynamic susceptibility contrast MRI in glioblastoma.** *Clin Neurol Neurosurg* 2012;114:607–12
9. Liu X, Tian W, Kolar B, et al. **MR diffusion tensor and perfusion-weighted imaging in preoperative grading of supratentorial nonenhancing gliomas.** *Neuro Oncol* 2011;13:447–55
10. Lee EJ, Lee SK, Agid R, et al. **Preoperative grading of presumptive low-grade astrocytomas on MR imaging: diagnostic value of minimum apparent diffusion coefficient.** *AJNR Am J Neuroradiol* 2008;29:1872–77
11. Yang D, Korogi Y, Sugahara T, et. al. **Cerebral gliomas: prospective comparison of multivoxel 2D chemical-shift imaging proton MR spectroscopy, echoplanar perfusion and diffusion-weighted MRI.** *Neuroradiology* 2002;44:656–66
12. Zou QG, Xu HB, Liu F, et al. **In the assessment of supratentorial glioma grade: the combined role of multivoxel proton MR spectroscopy and diffusion tensor imaging.** *Clin Radiol* 2011;66:953–60
13. Li X, Lu Y, Pirzkall A, et al. **Analysis of the spatial characteristics of metabolic abnormalities in newly diagnosed glioma patients.** *J Magn Reson Imaging* 2002;16:229–37
14. Di Costanzo A, Scarabino T, Trojsi F, et al. **Multiparametric 3T MR approach to the assessment of cerebral gliomas: tumor extent and malignancy.** *Neuroradiology* 2006;48:622–31
15. Law M, Yang S, Wang H, et al. **Glioma grading: sensitivity, specificity, and predictive values of perfusion MR imaging and proton MR spectroscopic imaging compared with conventional MR imaging.** *AJNR Am J Neuroradiol* 2003;24:1989–98
16. Weber MA, Zoubaa S, Schlieter M, et al. **Diagnostic performance of spectroscopic and perfusion MRI for distinction of brain tumors.** *Neurology* 2006;66:1899–906
17. Roy B, Gupta RK, Maudsley AA, et al. **Utility of multiparametric 3-T MRI for glioma characterization.** *Neuroradiology* 2013;55:603–13
18. Server A, Kulle B, Gadmar ØB, et al. **Measurements of diagnostic examination performance using quantitative apparent diffusion coefficient and proton MR spectroscopic imaging in the preoperative evaluation of tumor grade in cerebral gliomas.** *Eur J Radiol* 2011;80:462–70
19. Johannessen AL, Torp SH. **The clinical value of Ki-67/MIB-1 labeling index in human astrocytomas.** *Pathol Oncol Res* 2006;12:143–47
20. Guillevin R, Menuel C, Duffau H, et al. **Proton magnetic resonance spectroscopy predicts proliferative activity in diffuse low-grade gliomas.** *J Neurooncol* 2008;87:181–87
21. Yin Y, Tong D, Liu X, et al. **Correlation of apparent diffusion coefficient with Ki-67 in the diagnosis of gliomas.** *Zhongguo Yi Xue Ke Xue Yuan Xue Bao* 2012;34:503–08
22. Luh WM, Wong EC, Bandettini PA, et al. **QUIPSS II with thin-slice TI1 periodic saturation: a method for improving accuracy of quantitative perfusion imaging using pulsed arterial spin labeling.** *Magn Reson Med* 1999;41:1246–54
23. Fink JR, Carr RB, Matsusue E, et al. **Comparison of 3 Tesla proton MR spectroscopy, MR perfusion and MR diffusion for distinguish-**

ing glioma recurrence from posttreatment effects. *J Magn Reson Imaging* 2012;35:56–63
24. Magalhaes A, Godfrey W, Shen Y, et al. **Proton magnetic resonance spectroscopy of brain tumors correlated with pathology.** *Acad Radiol* 2005;12:51–57
25. Cha S, Knopp EA, Johnson G, et al. **Intracranial mass lesions: dynamic contrast-enhanced susceptibility-weighted echo-planar perfusion MR imaging.** *Radiology* 2002;223:11–29
26. Järnum H, Steffensen EG, Knutsson L, et al. **Perfusion MRI of brain tumours: a comparative study of pseudo-continuous arterial spin labelling and dynamic susceptibility contrast imaging.** *Neuroradiology* 2010;52:307–17
27. Aronen HJ, Gazit IE, Louis DN, et al. **Cerebral blood volume maps of gliomas: comparison with tumor grade and histologic findings.** *Radiology* 1994;191:41–51
28. Knopp EA, Cha S, Johnson G, et al. **Glial neoplasms: dynamic contrast-enhanced T2*-weighted MR imaging.** *Radiology* 1999;211:791–98
29. Kim MJ, Kim HS, Kim JH, et al. **Diagnostic accuracy and interobserver variability of pulsed arterial spin labeling for glioma grading.** *Acta Radiol* 2008;49:450–57
30. Sharma S, Sharma MC, Gupta DK, et al. **Angiogenic patterns and their quantitation in high grade astrocytic tumors.** *J Neurooncol* 2006;79:19–30
31. Calvar JA, Meli FJ, Romero C, et al. **Characterization of brain tumors by MRS, DWI and Ki-67 labeling index.** *J Neurooncol* 2005;72:273–80

Findings from positron emission tomography and genetic analyses for cerebellar liponeurocytoma

Hirokazu Takami, Akitake Mukasa, Masako Ikemura, Jyunji Shibahara, Miwako Takahashi, Toshimitsu Momose & Nobuhito Saito

Brain Tumor Pathology

ISSN 1433-7398

Brain Tumor Pathol
DOI 10.1007/s10014-014-0210-4

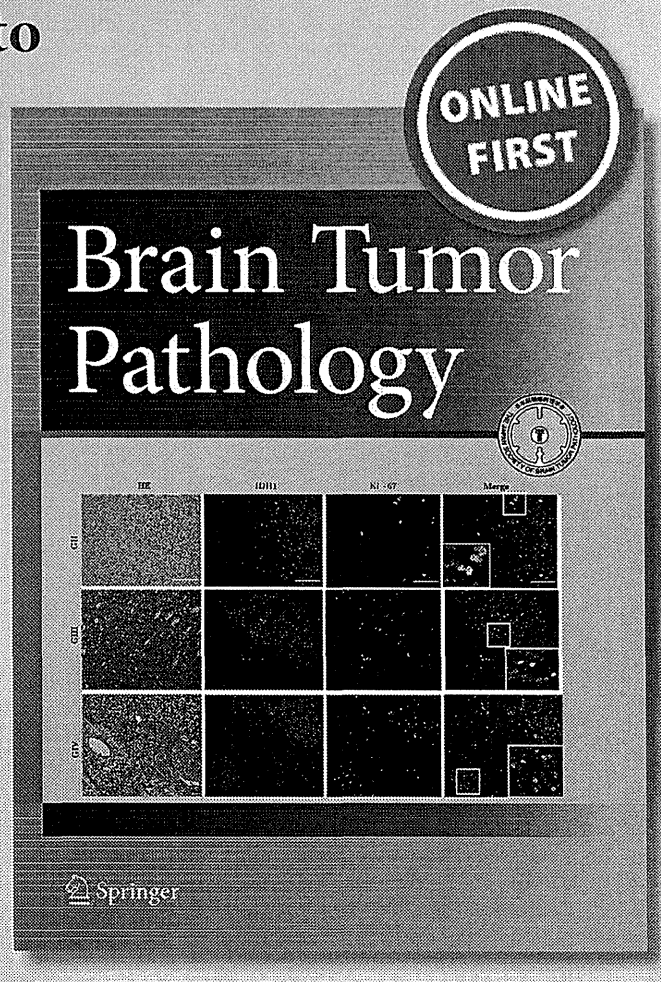

Springer

Brain Tumor Pathol
DOI 10.1007/s10014-014-0210-4

CASE REPORT

Findings from positron emission tomography and genetic analyses for cerebellar liponeurocytoma

Hirokazu Takami · Akitake Mukasa · Masako Ikemura · Jyunji Shibahara · Miwako Takahashi · Toshimitsu Momose · Nobuhito Saito

Received: 18 August 2014 / Accepted: 8 December 2014

Abstract Cerebellar liponeurocytoma is a rare tumor that usually develops in adult patients, and is categorized as World Health Organization grade II. Because of the small number of reports on its radiological and pathological features, the disease remains poorly characterized. The current case involved a 59-year-old man with tumor in the upper cerebellar vermis. Preoperative positron emission tomography (PET) showed high uptake on ^{11}C-methionine PET, but low uptake on ^{18}F-fluorodeoxyglucose PET. These findings resemble those of central neurocytoma and oligodendroglioma, but are incompatible with other brain tumors. Subtotal tumor removal was performed by suboccipital craniotomy. Histopathological examinations showed sheets of small, isomorphic cells with round nuclei and clear cytoplasm, and focal vacuolated cells resembling adipose cells. On immunohistochemistry, tumor cells were positive for synaptophysin and NeuN. Vacuolated cells were immunoreactive for perilipin. Based on these findings, cerebellar liponeurocytoma was diagnosed. Genetic analyses revealed absences of both chromosome 1p/19q loss and isocitrate dehydrogenase 1 mutation, further ruling out oligodendroglioma. These radiological and genetic aspects of cerebellar liponeurocytoma, which are mostly in common with central neurocytoma, should prove helpful in differentiating this rare tumor from other tumors with similar morphology.

Keywords Cerebellar liponeurocytoma · IDH · Immunohistochemistry · PET

H. Takami · A. Mukasa (✉) · N. Saito
Department of Neurosurgery, The University of Tokyo Hospital, 7-3-1 Hongo, Bunkyo-ku, Tokyo 113-8655, Japan
e-mail: mukasa-nsu@umin.ac.jp

M. Ikemura · J. Shibahara
Department of Pathology, The University of Tokyo Hospital, Tokyo, Japan

M. Takahashi · T. Momose
Department of Nuclear Medicine, The University of Tokyo Hospital, Tokyo, Japan

Introduction

Cerebellar liponeurocytoma is a rare neoplasm that was first introduced to the World Health Organization (WHO) classification in 2000 as a distinct clinicopathological entity among the central nervous system tumors [11]. In the 2007 WHO classification, cerebellar liponeurocytoma is defined as WHO grade II [14]. This neoplasm develops predominantly in the cerebellar hemispheres and vermis, and is characterized morphologically by focal lipidization within sheets of small, isomorphic round cells expressing both neuronal and glial markers [2, 9]. Cerebellar liponeurocytoma resembles neurocytoma microscopically, and expression profile analyses have also identified a close relationship to central neurocytoma [9]. Although findings from computed tomography (CT) and magnetic resonance imaging (MRI), pathological and immunohistochemical characteristics, and clinical behaviors have been reported in the literature [1, 4, 10], the characteristics of this tumor are still poorly understood. Because previous reports have demonstrated that patients with cerebellar liponeurocytoma usually show a favorable clinical course without adjuvant therapy after surgical removal [4, 10], accurate differential diagnosis of this rare pathology from other brain tumors is important in order to avoid unnecessary aggressive adjuvant therapies. However, differentiating neurocytoma and liponeurocytoma from other tumors such as oligodendroglial tumors, clear cell

Published online: 20 December 2014

ependymomas, dysembryoplastic neuroepithelial tumors (DNTs) and medulloblastomas is sometimes difficult under light microscopy, given the similar histological patterns such as perinuclear halo with round nuclei and cells [14]. We report herein an additional case, focusing on positron emission tomography (PET) findings and genetic perspectives that may prove useful in identifying this rare neoplasm.

Case report

A 59-year-old man visited the hospital after experiencing sporadic headaches and vertigo. Physical examination showed no neurological abnormalities. CT revealed an isodense to slightly hyperdense mass within the upper cerebellar vermis. The diameter of the mass was approximately 3.5 cm. MRI showed iso-intensity on T1-weighted imaging, heterogeneous intensity on T2-weighted imaging, high intensity on diffusion-weighted imaging, and slight hyperintensity on fluid-attenuated inversion recovery (FLAIR) imaging. Slight enhancement was observed after gadolinium administration (Fig. 1a–f). No feeding arteries were apparent on angiographic studies. To evaluate the metabolic activity of the tumor, radioisotope examinations were performed. Lower tumor accumulation was seen with ^{18}F-fluorodeoxyglucose (FDG) PET compared with normal cerebellar cortex, showing a lesion-to-normal cerebral cortex accumulation ratio (L/N) of 0.62, whereas the tumor showed higher accumulation on ^{11}C-methionine PET (L/N, 2.73) (Fig. 2a, b).

Preoperative differential diagnoses included anaplastic astrocytoma, oligodendroglial tumor, ependymoma, malignant lymphoma, and extraventricular neurocytoma. Since the tumor was relatively large in the posterior fossa, methionine PET demonstrated relatively high uptake, and diagnosis was difficult based solely on imaging examinations, we proceeded with surgical removal of the tumor by suboccipital craniotomy using a supra-cerebellar approach.

Under operative microscopy, the tumor showed generally whitish coloration, with moderate vascularity and mixed consistency. A clear cleavage plane was evident on the side of the cerebellar cortex, but no clear plane was seen on the side of the vermis, which was considered as the site of tumor origin. The patient was administered 5-aminolevulinic acid (5-ALA) preoperatively, resulting in no fluorescence at the tumor under violet–blue excitation light intraoperatively. Since the inferior vermian vein limited the operative approach, only subtotal resection could be achieved.

Histologically, the tumor comprised small, monomorphous cells with round nuclei and lightly eosinophilic to clear cytoplasm (Fig. 3a). Rare tumor cells showed intracytoplasmic vacuoles, reminiscent of lipid droplets (Fig. 3b). Mitosis was rarely observed. Immunohistochemical analysis was performed using a BenchMark XT automated immunostainer (Ventana Medical Systems, Inc., Tucson, AZ). Tumor cells were diffusely immunoreactive for synaptophysin (monoclonal, MRQ-40, Roche, Fig. 3c). Vacuolated cells were immunoreactive for perilipin, a lipid-droplet associated protein (polyclonal, Progen Biotechnik, Fig. 3d). Tumor cells were moderately stained for NeuN (monoclonal, MAB377, Merck Millipore, Fig. 3e). Immunoreactivity to GFAP was observed, largely on non-neoplastic astrocytes (monoclonal, 6F-2, Dako, Fig. 3f). Tumor cells were totally negative for Olig2 (polyclonal, IBL, Fig. 3g). Ki67-labeling index was 2 % (monoclonal, MIB-1, DAKO, Fig. 3h). On the basis of these histopathological findings, cerebellar liponeurocytoma was diagnosed.

To further confirm the differential diagnosis, genetic analyses were performed. Chromosome 1p and 19q co-deletion was not detected in the microsatellite analysis performed as described previously [29]. The presence of *IDH1* mutation was also denied by direct Sanger sequencing targeting codon 132 [17]. This genetic information indicated that oligodendroglial tumor was unlikely.

Although localized residual tumor was present on postoperative MRI, since the clinical course of cerebellar liponeurocytoma is generally reported to be slow and pathological features were benign in the current case, the patient was not treated with adjuvant therapy. At outpatient follow-up 2 years postoperatively, the small residual tumor showed no enlargement and the patient remained without any neurological disability.

Discussion

This case report suggests that preoperative PET and postoperative genetic analyses of tumor tissue might be useful for diagnosing liponeurocytoma.

Although PET findings for central neurocytoma have been documented in a small number of cases, findings for cerebellar liponeurocytoma have not been reported. Central neurocytoma generally shows low uptake on FDG-PET, reflecting low glucose metabolism [16, 27]. An exception was reported by Mineura et al., who described high uptake on FDG-PET for a tumor that showed regrowth 7 months after partial removal. Their report suggests that increased FDG uptake can be interpreted as predicting rapid tumor progression and a malignant prognosis [16]. On ^{11}C-methionine PET, central neurocytoma usually shows higher accumulation than normal cortex [16]. In a study of two cases of central neurocytoma by Takao et al. [27], L/N ratios as high as 1.68 and 2.80 were reported. In the current case, the

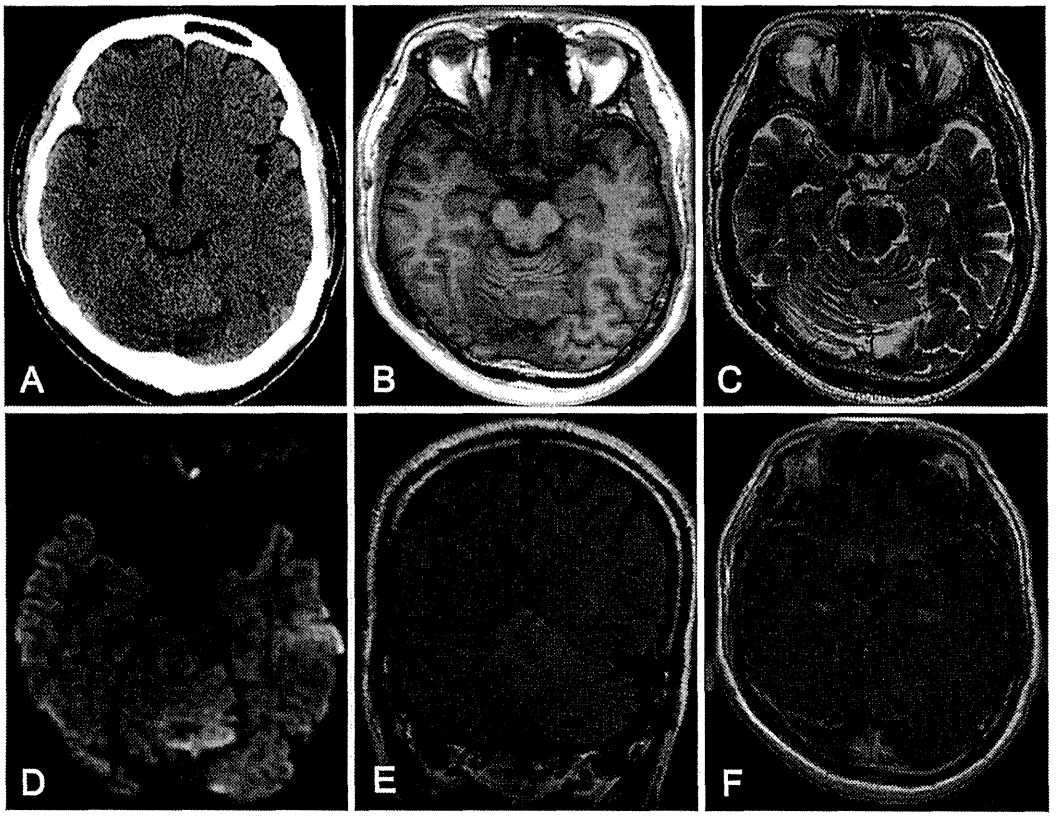

Fig. 1 Computed tomography (CT) and magnetic resonance imaging (MRI). **a** Axial CT, **b** T1-weighted axial MRI, **c** T2-weighted axial MRI, **d** diffusion-weighted axial MRI, **e** coronal fluid-attenuated inversion recovery MRI, **f** gadolinium-enhanced T1-weighted axial MRI. These images show a lesion measuring 3.5 cm in diameter in the upper cerebellum, with an indefinite boundary and without surrounding edema. Contrast enhancement is only slightly observed in the tumor

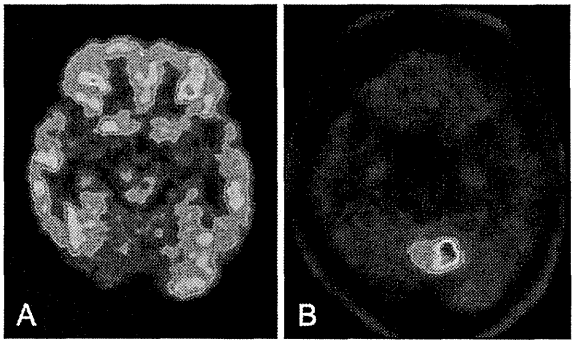

Fig. 2 Results for ^{18}F-fluoro-deoxy-glucose (FDG) (**a**) and ^{11}C-methionine (**b**) positron emission tomography (PET). Compared with normal cerebellar cortex, lower (L/N, 0.62) and higher (L/N, 2.73) accumulations are observed, respectively

tumor showed lower uptake on FDG-PET, but higher uptake on ^{11}C-methionine PET; these uncorrelated PET findings were consistent with previous observations of central neurocytoma, indicating that these two pathological entities may have similar metabolic traits.

Oligodendrogliomas also show somewhat similar findings on FDG and ^{11}C-methionine PET. In the study by Giammarile et al. [7], all 8 cases of oligodendroglioma showed a tumor/normal tissue ratio of around 1 (range 0.9–1.8) and higher accumulation (range 1.4–5.9) on FDG and methionine PET, respectively. Ependymomas and medulloblastomas tend to show higher uptake on both FDG and methionine PET [3, 8, 19, 28], whereas DNTs show lower and normal to slightly higher uptake compared with normal cortex on those studies, respectively [22]. These differences on FDG and methionine PET studies according to the differing histologies would help in preoperative diagnosis.

With regard to histopathological features, liponeurocytoma is a neurocytic neoplasm showing focal lipomatous change and astrocytic differentiation, evidenced by focal immunoreactivity to GFAP, which is also observed in most cases [14]. Immunohistochemical studies have indicated